Estuarine, Coastal and Shelf Science 259 (2021) 107446

Contents lists available at ScienceDirect

Estuarine, Coastal and Shelf Science

journal homepage: www.elsevier.com/locate/ecss

Geospatial distribution of hypoxia associated with a *Karenia brevis* bloom

Eric C. Milbrandt [a,*], A.J. Martignette [a], M.A. Thompson [a], R.D. Bartleson [a], E.J. Phlips [b], S. Badylak [b], N.G. Nelson [c]

[a] Marine Laboratory, Sanibel-Captiva Conservation Foundation, 900A Tarpon Bay Rd, Sanibel, FL, 33908, USA
[b] Fisheries and Aquatic Sciences, University of Florida, Gainesville, FL, USA
[c] Biological and Agricultural Engineering, North Carolina State University, Raleigh, NC, USA

ARTICLE INFO

Keywords:
Caloosahatchee
phytoplankton
stratification
hypoxia
red tide

ABSTRACT

In 2018, the presence of bottom water hypoxia along the SW Florida coast was investigated during a bloom of the toxic dinoflagellate *Karenia brevis*. The bloom was first detected in November 2017. Monitoring of oxygen levels and bloom densities was carried out in 2018 and 2019 using sampling grids. Vertical profiles indicated a pycnocline at 3–4 m where warmer, lower salinity water was at the surface, while the deeper hypoxic layer was colder with higher salinity. There were significantly higher abundances of *K. brevis* in the surface water compared to the hypoxic bottom water in September 2018. At two fixed sites, dissolved oxygen was measured continuously showing hypoxic conditions during that month. Geospatial analysis of vertical profile data yielded an estimate that the hypoxic layer covered an area of at least 655 km^2. The possible influences of red tides on hypoxic conditions along the coast of the eastern Gulf of Mexico are discussed within the context of the 2018 *K. brevis* bloom event. Hypoxia occurring in parallel to a red tide bloom is more likely to occur with warmer ocean temperatures and increased fluxes of nutrients and fresh water to the Gulf of Mexico after hurricanes.

1. Introduction

The combination of global climate change and increasing cultural eutrophication will likely exacerbate the incidence and intensity of harmful algal blooms and hypoxic events (Anderson et al., 2002; Heisler et al., 2008; Paerl and Paul, 2012; Griffith and Gobler, 2020; Phlips et al., 2020). Coastal regions can be subject to hypoxic conditions due to intense harmful algal blooms (HABs) that result in high biological oxygen demand, particularly as blooms collapse and decompose (Howarth et al., 2011). Although hypoxia is widely understood to disrupt coastal ecosystems, research on the extent of hypoxic conditions remains limited and the role of hypoxia is often overlooked unless it impacts higher trophic levels (Diaz and Rosenberg, 2008). One of the more extensively studied examples of hypoxia associated with HABs is the nearshore region of the Mississippi River discharge in the northern Gulf of Mexico, often referred to as the "dead zone" (Rabalais and Turner, 1994; Rabalais et al., 2014, Zhang et al., 2010).

Along the broad continental shelf environment of the eastern Gulf of Mexico, another potential cause of hypoxia is a red tide bloom. These blooms can extend over thousands of square kilometers and impact coastal regions all along the west coast of Florida. Red tide blooms in the eastern Gulf of Mexico frequently occur during the late summer and are most often dominated by the toxic dinoflagellate *Karenia brevis* (Tester and Steidinger, 1997; Vargo et al., 1987; Heil et al., 2014a). *Karenia brevis* produces brevetoxins, which can impact marine fauna, leading to mass mortalities (Fire et al., 2007; Landsberg et al., 2009). In turn, these mortalities, bacterial decomposition of the biomass, and the presence of high *K. brevis* biomass interact to create opportunities for the formation of low oxygen zones, particularly during periods of vertical water column stratification. Periods of low winds and increased solar heating during the summer can cause vertical stratification which results in the formation of a thermocline, and enhanced potential for hypoxia (He and Weisberg, 2002). Two studies of nearshore benthic and reef communities in the Eastern Gulf of Mexico before and after red tide events attributed mortality not only to exposure to brevetoxins, but also the effects of oxygen depletion, hydrogen sulfide poisoning and bacterial infections (Smith, 1975). These events can disrupt climax communities and re-structure epibenthic and fish communities for 2–3 years. The expectation is that deoxygenation of the oceans will be exasperated by climate change in areas with recurring HABs (Gobler et al., 2017; Griffith and Gobler, 2020).

In this study, a widespread hypoxia event in 2018 associated with a red tide is described along the southwest coast of Florida. The impacted region is part of the shallow West Florida Shelf (WFS) which extends

* Corresponding author.

https://doi.org/10.1016/j.ecss.2021.107446
Received 1 February 2021; Received in revised form 21 May 2021; Accepted 27 May 2021
Available online 4 June 2021

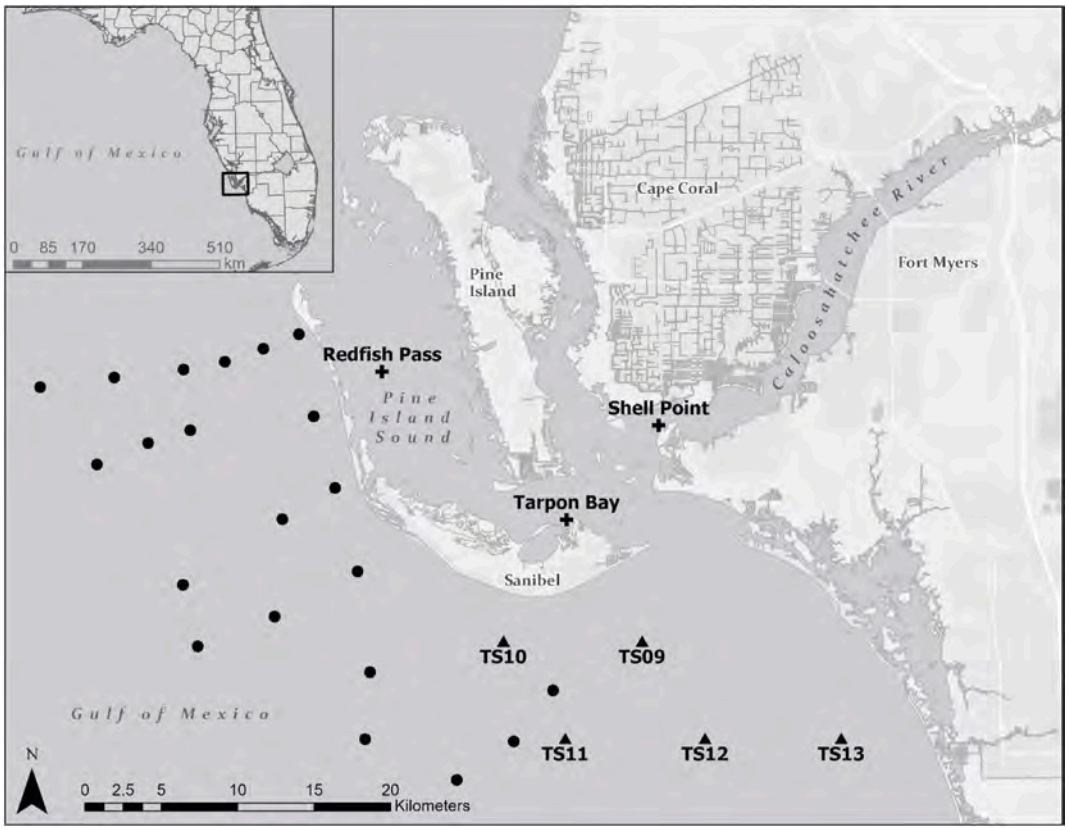

Fig. 1. Map of the study area. Water column profile sites (circles) to collect salinity, temperature, and dissolved 2 oxygen visited on three separate cruises. Similar data were collected at TS09-TS13 (triangles) from Sept. 3 2018 to Nov. 2018. Wind speed data and continuous dissolved oxygen and depth during the hypoxic event were collected at the sites 4 identified as plus symbols.

over 250 km from shore in the eastern Gulf of Mexico (Weisberg et al., 2009). Along the coast, red tides are concentrated in shallow water by wind and currents resulting in elevated plankton biomass levels (Vargo, 2009). The red tide was first detected in November 2017 and partially mapped with an autonomous sailing vessel (Beckler et al., 2019). Hypoxia was found in a large area in the Gulf of Mexico in August and September 2018. The primary goals of the study were to characterize physicochemical conditions, including the intensity and geospatial distribution of hypoxia in parallel with concentrations of the dominant species, *K. brevis*. Specific study objectives included (1) monitoring physicochemical covariates and *K. brevis* levels across multiple depths and locations in waters impacted by the red tide, and (2) quantifying the severity and extent of hypoxia as a function of *K. brevis* concentrations and physicochemical conditions. Findings from this work provide new insights into the ecological impacts associated with the interactions of harmful algal blooms and hypoxia.

2. Materials and methods

The study area encompassed approximately 1200 km^2, with relatively shallow depths ranging from 5 m to 20 m (Fig. 1). Sampling was initiated in September 2018 in response to an unusual mass mortality of fish and benthic invertebrates. A network of water sampling sites was established to determine the extent and severity of hypoxia in the study region. The network included three major components:

1) Three sampling cruises (09/26/2018, 10/29/2018, 09/17/2019) involving 21 sites (Fig. 1, solid circles) to provide the spatial scale during hypoxia. Eight transects were positioned approximately 7.5 km apart perpendicular to shore. Transects were approximately 20 km long with 4–6 stations per transect. This approach was based on previous hypoxia research in the Northern Gulf of Mexico (Rabalais et al., 2007) and NOAA guidance (T. Meckley, pers. comm). A profile of key water column parameters and discrete water samples were collected for microscopic detection of phytoplankton, including *Karenia brevis*.
2) Time series (TS) sampling events were carried out at five sites (Fig. 1, filled triangles) from September 2018 to November 2019.
3) Continuous monitoring of water column characteristics at two fixed platforms (Fig. 1, Tarpon Bay and Shell Point), where hourly measurements were made with environmental probes.

Water physical, optical and dissolved oxygen measurements. At all stations, an EXO2 sonde connected to an EXO Handheld (Yellow Springs Instruments, Ohio) with a 25 m cable was lowered to 0.5 m off the bottom. The handheld was set to rapid, continuous mode and sampled at 1 Hz. The sonde was brought up through the water column at a rate of 2 m min^{-1} for dissolved oxygen, salinity, temperature, *in situ* chlorophyll-*a* (chl *a*), fluorescent dissolved organic matter (FDOM), turbidity and pH. Probes were calibrated prior to each sampling event according to manufacturer's recommended standards (Yellow Springs Instruments, Ohio).

For the five time-series stations (TS09-TS13), discrete water samples were collected from the surface and bottom of the water column. Water from the upper 2 m was collected with a 2 m (5 cm diameter) integrating pole to avoid biasing of samples due to vertical layering of phytoplankton populations (Phlips et al., 2012). Three samples (upper 2 m) were placed into a pre-washed 18 L bucket. A 125 mL screw amber glass bottle was filled for phytoplankton analysis and preserved with 2 mL of Lugols fixative. A second 22 mL glass vial was filled for picoplankton analysis and 0.4 mL of 40% glutaraldehyde was used to preserve the sample. In addition, 1000 mL of water from the integrated sample was

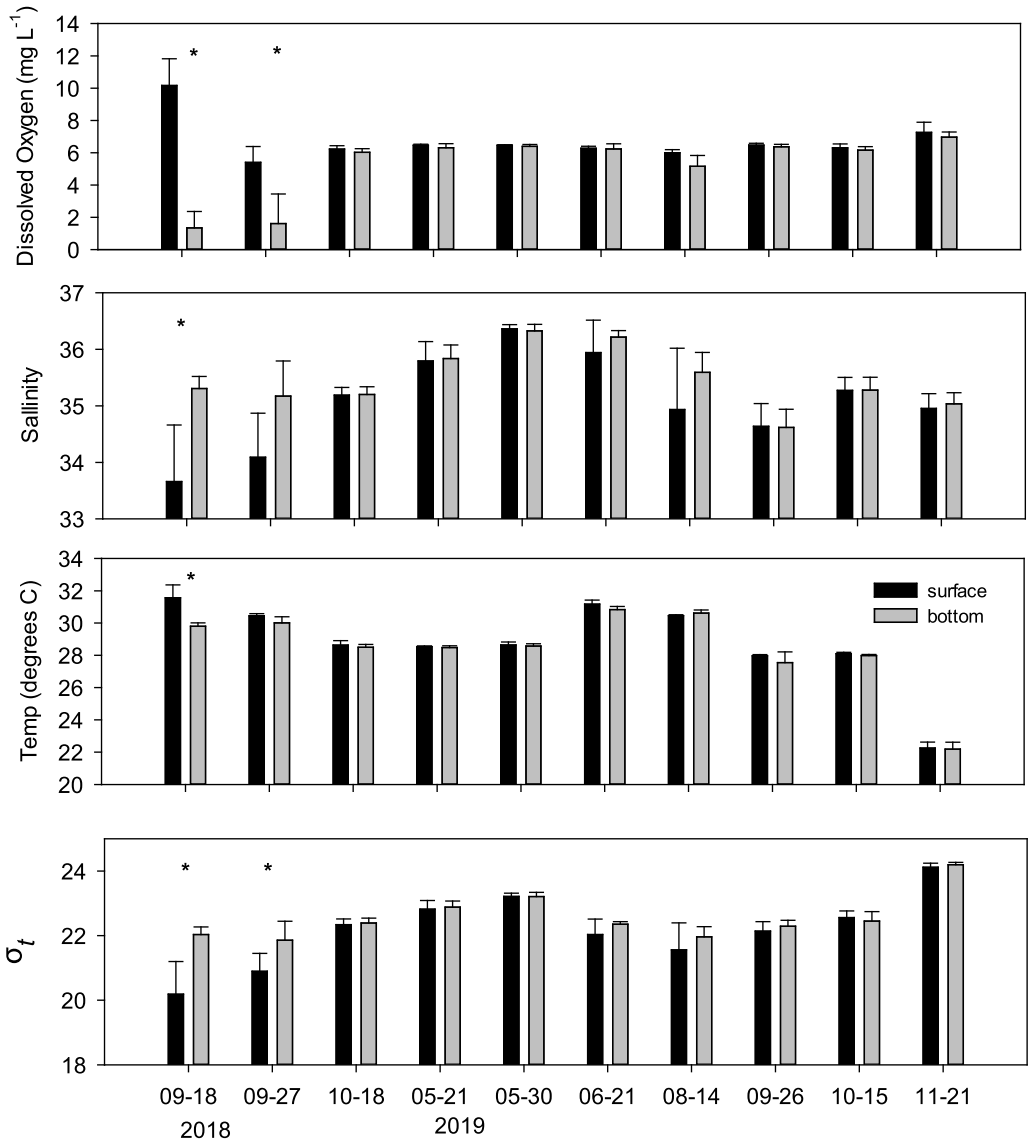

Fig. 2. Mean dissolved oxygen, salinity (empirical), temperature (empirical) and density (calculated) at 9 sites TS09-TS13 (triangles). Error bars are +1 s.d. Asterisks (*) represent statistically significant 10 differences between surface and bottom samples (n = 5 sites).

filtered onto 0.7 μm 47 mm glass-fiber filters (Millipore GF/F). A filter was collected for chlorophyll *a* and pheophytin analysis according to Standard Methods, after extraction in 95% ethanol (EPA Method 445.0). Bottom samples were collected using a Van Dorn sampling bottle (2 L) deployed to 0.5 m above the bottom. The sample was place into the pre-rinsed bucket and phytoplankton samples were collected as described. All samples were placed in a cooler with ice packs for transportation back to the laboratory.

Phytoplankton species identification and enumeration. Phytoplankton community composition samples were analyzed using light and fluorescence microscopy. Phytoplankton composition was determined using the Utermohl method (Utermöhl, 1958). Lugols preserved samples were settled in 19 mm (inside diameter) cylindrical chambers. Phytoplankton cells were identified and counted at 100 × and 400 × magnification with a Nikon phase contrast inverted microscope. At 400 × , a minimum of 100 cells of a single taxon and 30 grids were counted. If 100 cells were not counted by 30 grids, up to a maximum of 100 grids were counted until 100 cells of a single taxon was reached. At 100 × a total bottom count was completed for taxa greater than 30 μm and converted to carbon units (Menden-Deuer and Lessard, 2000).

Geospatial modeling of dissolved oxygen concentrations. Geospatial modeling was performed to estimate the volume of water impacted by the hypoxic zone in the study area. Based on Vaquer-Sunyer and Duarte (2008) review showing sublethal effects to many taxa occurring from 0 to 3 mg L^{-1}, the model results were grouped into hypoxia (0–3 mg L^{-1}), normoxia (3–8 mg L^{-1}) and supersatured (>8 mg L^{-1}). Geographic information system (GIS) was used to determine a 3-dimensional model of dissolved oxygen concentrations from sites in the study area. There was an existing tool within ESRI ArcGIS that used empirical data to provide a 3-D model of the water column (Krivorucho and Gribov, 2019). All dissolved oxygen data (mg L^{-1}) from the profiles conducted on 09/26/18 were imported into ESRI ArcGIS Pro (ver. 2.3). Empirical Bayesian Kriging 3D (EBK3D), was used to interpolate the water column profiles into a three-dimensional model of dissolved oxygen levels. A log transformation was applied to correct for the data being skewed towards low DO values and a first order trend removal to correct for a vertical trend. The optimal Elevation Inflation Factor was determined by the EBK3D tool. Two dimensional layers were classified into 1 mg L^{-1} ranges and exported at 0.5 m depth intervals. The layers were clipped to area using bathymetry shapefiles. The surface area by class range was calculated for each layer. The sum of the areas was multiplied by 0.5 (the depth between each layer) to estimate the total

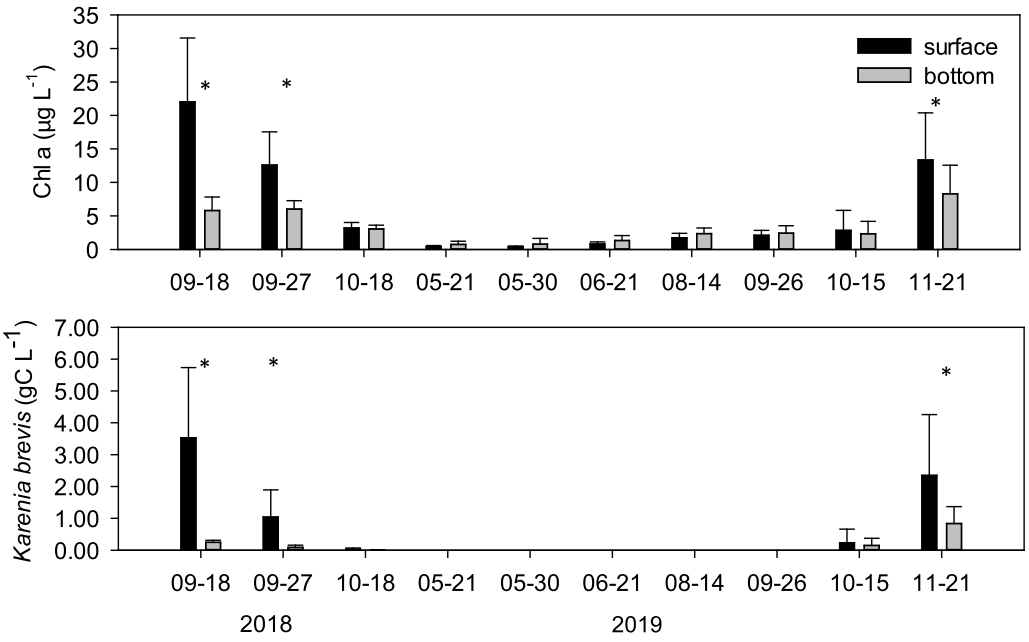

Fig. 3. Mean Chlorophyll *a* and *Karenia brevis* abundances during a series of discrete sampling events. 14 Error bars are +1 s.d. Asterisks (*) represent statistically significant differences between surface and 15 bottom samples (n = 5).

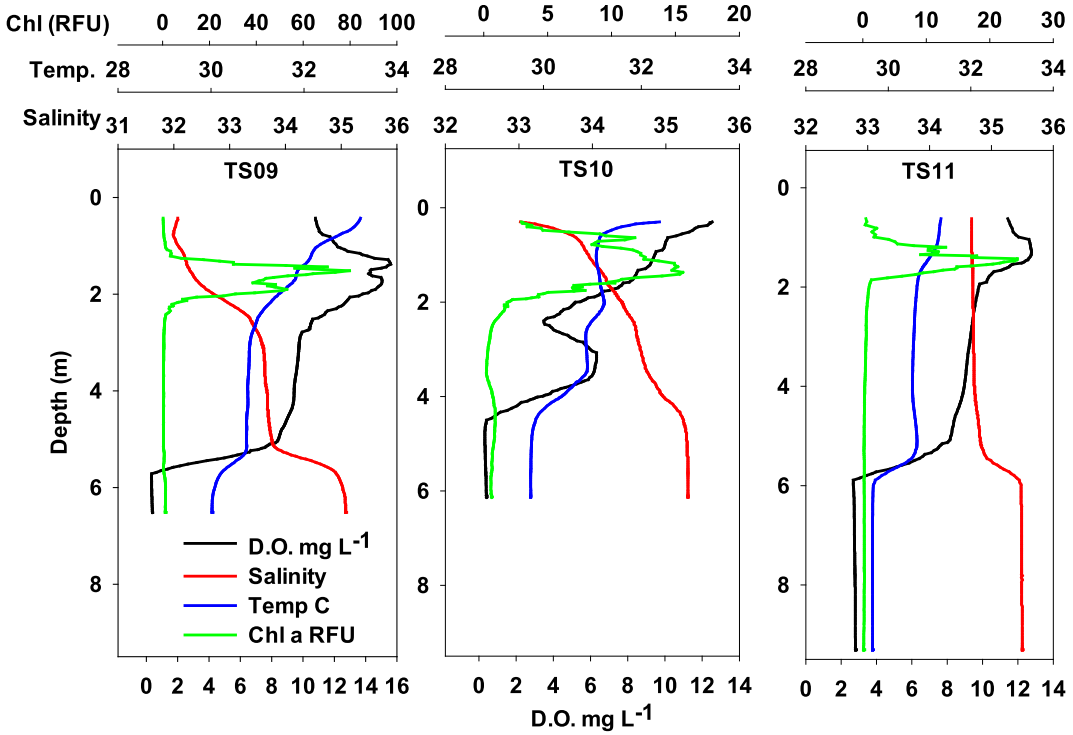

Fig. 4a. Vertical profiles from 09/18-18 during the lowest dissolved oxygen concentrations observed 19 during the study. Site names correspond to the map in Fig. 1. Chlorophyll *a* (RFU) shows peaks near the 20 surface (0–2 m), a characteristic of *K. brevis,* later confirmed by microscopy.

volume per class range. The EBK3D had a Continually Ranked Probability Score of 0.04 and a Root Mean Square Error of 0.14, suggesting that the error in dissolved oxygen concentrations within the model was low. Estimating volume from each depth slice was done because of the irregular shape of the 3D model due to changes in depth moving inshore to offshore. Volume estimates were important for comparison to other hypoxia areas.

Continuous monitoring at fixed platforms - Two fixed, hourly autonomous sites that are part of the Sanibel-Captiva Conservation Foundation River, Estuary and Coastal Observing Network (RECON; http://recon.sccf.org) provided continuous measurements. Data are also available at the Gulf of Mexico Coastal Ocean Observing System (GCOOS) data portal. At sites Tarpon Bay and Shell Point (plus symbols Fig. 1), there is a Seabird Land-Ocean Biochemical Observatory (Jannasch et al., 2008). This instrument package consists of a Water Quality Monitor (WQM) pumped Conductivity Temperature Depth (CTD) with a fluorometer used to collect salinity, temperature, depth, dissolved oxygen, *in situ* chlorophyll *a*, and turbidity. The instruments

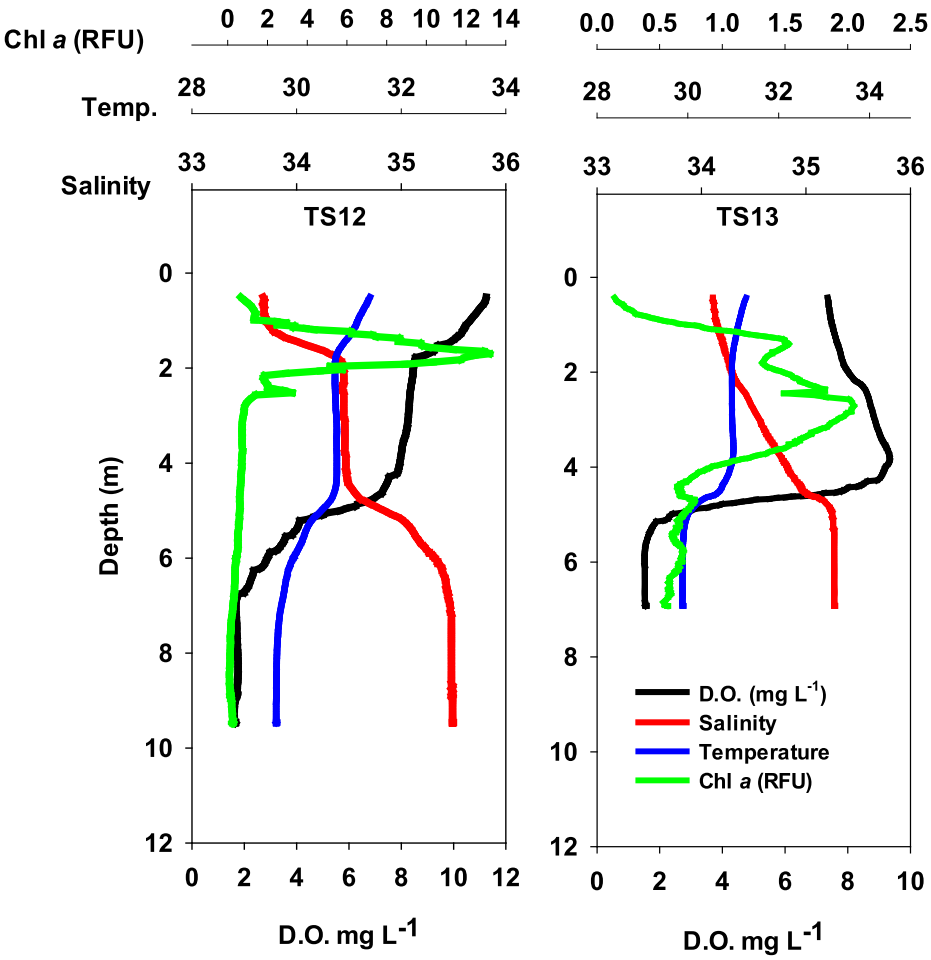

Fig. 4b. Vertical profiles from 09/18/21 during the lowest dissolved oxygen concentrations observed 24 during the study. Site names correspond to the map in Fig. 1.

were maintained and cleaned monthly.

Statistical analysis. Seawater densities were calculated following Millero et al. (1980). All of the time-series (TS) discrete samples were analyzed using MINTAB (ver. 13.2) to obtain descriptive statistics. For comparisons of surface versus bottom water, a paired *t*-test was used with the assumption of equal variances. Surface and bottom data were tested with Kolmogorov-Smirnov Normality test and Levene's test of equal variances. Data that were not normally distributed or did not have equal variances were compared using a Mann-Whitney nonparametric test. A Pearson correlation analysis was performed on salinity versus density. A Pearson correlation analysis was also used to evaluate the relationship between sensor depth and dissolved oxygen concentration during spring and neap tide cycles from the Shell Point RECON site.

3. Results

Water physical, optical, dissolved oxygen and phytoplankton species. The first detection of *Karenia brevis* was reported in October 2017 by the Florida Wildlife Research Institute (FWRI) through routine discrete sampling (https://myfwc.com/research/redtide/). The weekly FWRI monitoring program tracked the expansion of the bloom in low, medium and high ($>10^6$ cells L^{-1}) concentrations throughout the event. High concentrations of *Karenia brevis* were detected at many locations in July 2018 and the first measurement of hypoxia was in August 2018.

At five-site time-series (TS) sites (Fig. 1) sampling started on 09/18/18. Comparisons of mean values for surface and bottom data are shown in Figs. 2 and 3. Dissolved oxygen concentrations were significantly lower in the bottom water (1.34 mg L^{-1}) than surface water (10.16 mg L^{-1}) on 09/18/18 ($t = 11.00$, $df = 8$, $p < 0.05$). Similarly, on 09/27/28, dissolved oxygen was significantly lower at the bottom (1.61 mg L^{-1}) than the surface (5.40 mg L^{-1}; $t = 5.19$, $df = 8$, $p < 0.05$). Along with significantly lower dissolved oxygen in the bottom than surface water on 09/18/18, pH was significantly lower in the bottom water ($t = 7.69$, $df = 7$, $p < 0.05$). Bottom water salinity was significantly higher ($t = 4.47$, $df = 8$, $p < 0.05$) and temperature significantly lower (Mann-Whitney, $p < 0.05$) than in surface water on 09/18/18. Density was significantly higher in bottom than surface water ($t = 3.97$, $df = 8$, $p < 0.05$). Density remained significantly higher in the bottom water on 09/27/18. By the 10/18/18 sampling event, there was no evidence of a strong pycnocline, and the water column was not hypoxic. Hurricane Michael passed through the eastern Gulf of Mexico from October 8–10 and recorded 1.5 m wave heights for 24 h (RECON, http://recon.sccf.org/). Neither stratification nor hypoxia was observed in subsequent sampling events through 2019.

The highest extracted chlorophyll *a* concentration was 29.2 μg L^{-1} collected near the surface on 09/18/18, but in general mean chlorophyll *a* concentrations (Fig. 3) were higher in surface water (22.0 μg L^{-1}) than in bottom water (5.8 μg L^{-1}), ($t = 3.07$, $df = 4$, $p < 0.05$). Pheophytin was higher in the surface water on 09/18 (surf: 6.72 μg L^{-1}; btm: 2.25 μg L^{-1} and higher in bottom water on 09/27 (surf: 3.58 μg L^{-1}; btm: 5.48 μg L^{-1}). The dominant taxon was the toxic dinoflagellate *Karenia brevis* (Fig. 3) in samples collected on 09/18/18 and 09/27/18 and 11/21/19. The highest individual site biomass value for *K. brevis* was 6.03 g C L^{-1} (5,200,000 cells L^{-1}) at Site TS12 surface on Sept. 18, 2018. The chlorophyll *a* concentrations at TS12 in the surface was 26.0 μg L^{-1}. *Karenia brevis* biomass was higher in surface (3.52 g C L^{-1}) than bottom

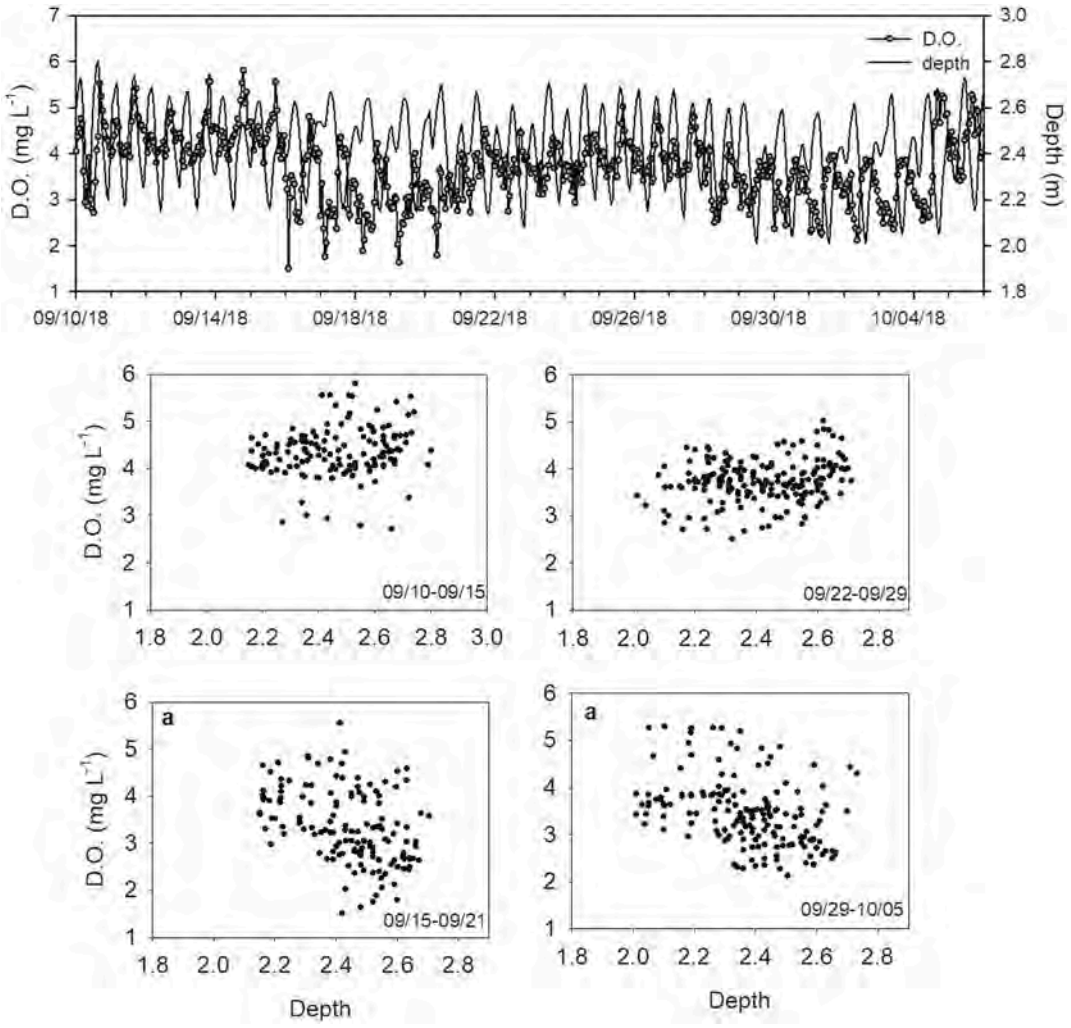

Fig. 5. (Upper) Time-series plot of dissolved oxygen and depth from Shell Point, a fixed sensor at 2 m 28 depth in foodnig spring tides (09/15–09/21; 09/29–10/05). (lower) Relationship between dissolved oxygen 29 and depth of water column. A significant negative correlation is indicated by (**a**).The low D.O. water 30 mass was being transported in during flood tides.

water (0.24 g C L^{-1}) on 09/18/18 (Mann Whitney, $p < 0.05$). *Karenia brevis* was also higher in surface samples in the 09/27/18 samples (Mann Whitney, $p < 0.05$). By 10/18/18, *K. brevis* was still present but at lower concentrations in all samples (Fig. 5). *Karenia brevis* was not present until it was found on 09/26/19. The bloom occurred until the final sampling event on 11/21/19. *Karenia brevis* was higher in the surface at TS sites on 09/26/19, 10/15/19, and 11/21/19 but not statistically significant. There were no differences in dissolved oxygen, salinity, temperature between surface and bottom samples in 2019.

Profiles of the water column at TS sites on 09/18/18 show the depth of the pycnocline caused by differences in salinity and temperature (Fig. 4a, b). Temperatures in the hypoxic bottom water were less than 30 °C and salinities were greater than 35 at all TS sites sampled on 09/18/18. Salinity and temperature profiles indicate the differences in surface and bottom layers at 4–5 m depth. Dissolved oxygen concentrations were below 2 mg L^{-1} in the lower layer. The hypoxic layer was low *in situ* chlorophyll *a* (Relative Fluorescent Units; RFU). This is in contrast to the warmer, lower salinity in the surface water layer. *In situ* chlorophyll *a* was high in surface waters and phytoplankton biomass was dominated by *K. brevis* (Fig. 3). The depth of the pycnocline varied slightly among sites but was around 2 m. There was a consistent decrease in dissolved oxygen concentration at the beginning of the pycnocline regardless of total depth, with hypoxic water present in the bottom layer (Fig. 4A, B).

Geospatial modeling of dissolved oxygen concentrations. To estimate the spatial extent of the hypoxia, all YSI profiles from geospatial grid sites (Fig. 1, filled circles) from a 09/26/18 cruise were modeled. Dissolved oxygen concentrations in the study area ranged from 0.27 mg L^{-1} to 11.35 mg L^{-1}. The dataset from 09/26/18 had the most data points collected in the same day when very low dissolved oxygen values were recorded. The model results are shown in Fig. 6 separated into 3 generalized dissolved oxygen categories; hypoxic (0–3 mg L^{-1}), normoxic (3–8 mg L^{-1}) and supersaturated (8–12 mg L^{-1}). The dissolved oxygen at 1 m depth slices shows that hypoxic conditions were in the deeper layer under a normoxic upper layer. Similar to the results from TS sites sampled on 09/18/18, the hypoxic layer was typically at depths greater than 4 m. However, at shallower sites nearshore, there was hypoxia at depths from 2 to 4 m. From the surface to 2 m there were also areas of supersaturation (Fig. 6). A large area in the south of the study area was supersaturated at the surface and corresponded with high *K. brevis* biomass.

The total estimated area of the hypoxic zone was estimated by calculating the area of dissolved oxygen concentrations at 0.5 m depth increments (Table 1). The total surface area of the study area was 683 km^2. Table 1 estimates the total area of each depth within the EBK3D model. For dissolved oxygen concentrations between 2 and 3 mg L^{-1}, the area was a small area (1 km^2) area from depths of 0.5–3.0 m. The area of the hypoxic layer at 5.0 m was 655 km^2 (Table 1) or 96% of the

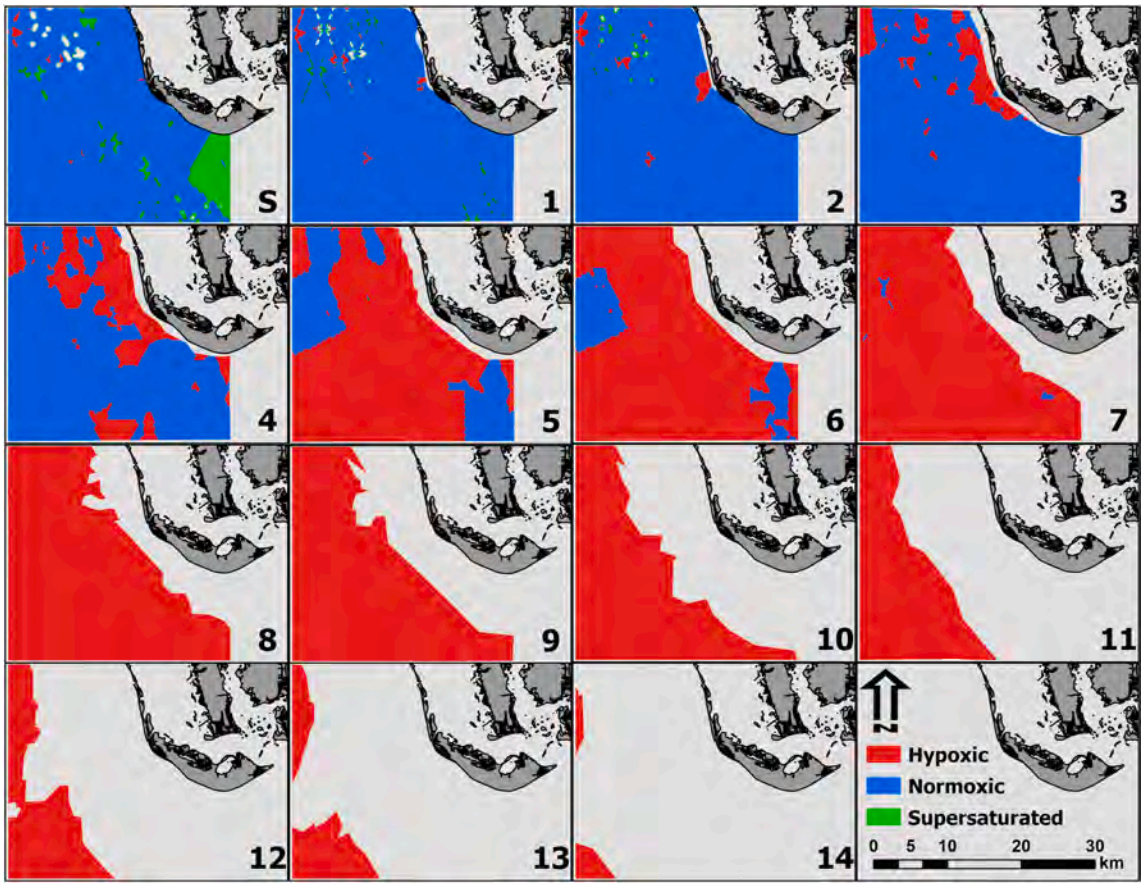

Fig. 6. Results from a 3-D model of dissolved oxygen in the water column based on YSI EXO2 sonde 34 vertical profile data collected on 09/26/18. Each tile is depth (m) and represents the dissolved oxygen 35 concentration from slices of the water column. Hypoxia is defined as 0–3 mg L-1, normoxia is 3–8 mg L-1 36 and supersaturated is 8–12 mg L-1. The total area for each slice can be found in Table 1. Light grey is the 37 sea floor.

area sampled. The total volume of the area sampled was 6.99 km^3 (Table 2). The volume of the hypoxic water was estimated to be 2.77 km^3 (Table 2) and represented 40% of the study area on 09/26/18. There was 0.07 km^3 or 1% that was supersaturated.

Continuous monitoring at fixed sites - Low oxygen conditions were also recorded at two fixed continuous monitoring platforms at Shell Point and Tarpon Bay in the lower estuary. Several low oxygen periods occurred during spring flood tides at Shell Point (Fig. 5). Low dissolved oxygen concentrations were found during successive flood tides from 09/15/18–09/21/18 and again from 09/29/18–10/05/18. Dissolved oxygen was negatively correlated with depth during spring tides 09/15/18-09-27/18 (Pearson correlation, -0.414, $p < 0.01$) and 09/29/18–10/06/18 (Pearson correlation, -0.393, $p < 0.01$) but not correlated during neap tides (Pearson correlation, 0.159, ns). At a different fixed site in the lower estuary, Tarpon Bay, there was a single flood tide when a low dissolved oxygen water mass was transported past the sensor. However, a typical diurnal pattern for dissolved oxygen concentration at Tarpon Bay was minimum values occurring at dawn and/or at low tide.

4. Discussion

Over the past two decades, much of the attention on marine hypoxia has focused on large-scale persistent or recurring phenomena, such as the 18,000 km^2 "dead zone" associated with the Mississippi River discharge (Rabalais and Turner, 1994; Scavia et al., 2003; IWG-HABHRCA, 2016), coastal upwelling of deep low oxygen water, and recurring hypoxia associated with intense cyanobacteria blooms in lakes, such as Lake Erie (Scavia et al., 2014; Smith et al., 2015; IWG-HABHRCA, 2016; Watson et al., 2016). The task of defining the potential for hypoxia in shallow and predominantly polymictic environments, such as the nearshore west Florida shelf, is complicated by the stochastic and spatially dynamic nature of blooms, such as red tide events involving *Karenia brevis* (Heil et al., 2014a). Many types of harmful algal blooms can be monitored with remote sensing technologies, such as satellite imagery (e.g., Barnes et al., 2014, Urquhart et al., 2017) or generally documented through *in situ* measurements and discrete sampling. The extensive hypoxic event observed in this study highlights how coastal red tides can co-occur with hypoxia and cause widespread impacts given the right conditions.

Two coinciding conditions likely set up the hypoxia event in WFS region in 2018, namely, (1) the development of a protracted period of water column stratification and calm wind conditions (Fig. 7) and fresh water discharges in 2018 (Fig. 8) and (2) the influx and development of an intense, toxic red tide bloom (*Karenia brevis*) in the region. The observed size of the hypoxia was greater than 600 km^2, however, the actual size of the hypoxia likely extended further into the Gulf of Mexico beyond the study region, as set by the locations of the sampling sites. A persistent pycnocline was observed at all sites indicating limited mixing of the bottom water with the surface water. In addition to calm wind conditions, high fresh water runoff from Peace, Myakka, and Caloosahatchee Rivers associated with a period of elevated rainfall likely enhanced the potential for stratification, and increased loading of particulate and dissolved organic carbon to the region, as observed in previous years (Milbrandt et al., 2010). Biological oxygen demand (BOD) in the lower water column and sediments were not measured in this study, but other studies have shown high oxygen demand can occur in the bottom waters subject to high carbon loads (Tomasko et al., 2006; CENR, 2010). Stratification plays an important role in hypoxic zones in

Table 1
Area corresponding to a given depth or dissolved oxygen concentration derived from the ArcGIS Empirical Bayesian Kriging 3D modeling tool. Hypoxia and anoxia was found in the deeper layer at depths greater than 2.5 m. The area was calculated from each depth from the model (see Fig. 4), extrapolated and then used to calculate a total volume estimate.

Depth (m)	Dissolved Oxygen (mg L^{-1})												
	<1	1–2	2–3	3–4	4–5	5–6	6–7	7–8	8–9	9–10	10–11	11–12	Area (km^2)
0.0			0	4	44	377	157	41	17	40	3	2	683
0.5			1	5	98	355	136	35	45	3	2	1	680
1.0			1	7	98	419	93	55	4	3	1	1	681
1.5			1	9	124	435	65	41	4	1	1	1	681
2.0			0	14	141	434	87	4	2	1	1	1	684
2.5			1	40	253	355	25	4	1	1	0	0	680
3.0			1	60	454	133	18	2	1	0	0		668
3.5			5	87	474	102	6	0	0				674
4.0			17	145	391	108	2						664
4.5		0	31	367	168	95	0						662
5.0		0	85	418	125	27							655
5.5		20	162	322	132	2							638
6.0		34	382	141	82	0							639
6.5	0	101	398	76	52								627
7.0	16	271	189	98	3								577
7.5	87	314	97	39	41								578
8.0	161	282	47	68									558
8.5	176	229	39	52									497
9.0	174	218	39	43									474
9.5	168	170	28	31									397
10.0	201	116	57										375
10.5	204	41	46										291
11.0	208	24	44										275
11.5	140	9	44										193
12.0	123	35	13										171
12.5	74	24	11										110
13.0	69	20	11										100
13.5	36	11	7										53
14.0	17	5	3										24
14.5	12	3	2										17
													14,006
Est. Volume (km^3)	0.93	0.96	0.88	1.01	1.34	1.42	0.29	0.09	0.04	0.02	0.00	0.00	6.99

Table 2
Volume estimates and percent of the total for each category of dissolved oxygen concentrations.

D.O. Range	Estimated Volume (km^3)	Percent of Total
Hypoxic (0–3 mg L^{-1})	2.77	39.63%
Normoxic (3–8 mg L^{-1})	4.15	59.37%
Supersaturated (8–12 mg L^{-1})	0.07	1.00%
Total	6.99	

other regions of the Gulf of Mexico, particularly where the difference between surface- and bottom-water salinities is greater than 4.1 (Stow et al., 2005). Such conditions have been observed in eutrophic estuaries (Howarth et al., 2011; Kemp et al., 2005), and have been linked to hurricane-associated runoff in nearby Charlotte Harbor (Tomasko et al., 2006; Turner et al., 2006). The hypoxia dissipated in October 2018 when tropical storm Michael impacted the eastern Gulf of Mexico, producing high winds, seas and strong coastal circulation.

The role of the *K. brevis* blooms in hypoxia included both direct and indirect impacts. Intense harmful algal blooms (HABs) can result in regional hypoxia due to high biological oxygen demand created by both the respiratory demand of the live bloom itself and decomposition of senescing bloom biomass (CENR, 2010; IWG-HABHRCA, 2016; Pitcher and Probyn, 2016). The direct effect is the respiratory demand of the bloom's biomass during senescence. However, two observations suggest that the peak biomass levels encountered in the *K. brevis* bloom of 2018 were likely not high enough to be the sole driver of hypoxia. Two studies of bloom-related hypoxia, one in coastal South Africa (Pitcher and Probyn, 2016) and one in the St. Lucie estuary in east Florida (Phlips et al., 2012, Phlips et al., 2015), involved surface water biomass levels of 100–1200 μg chlorophyll *a* L^{-1}, significantly higher than the peak values

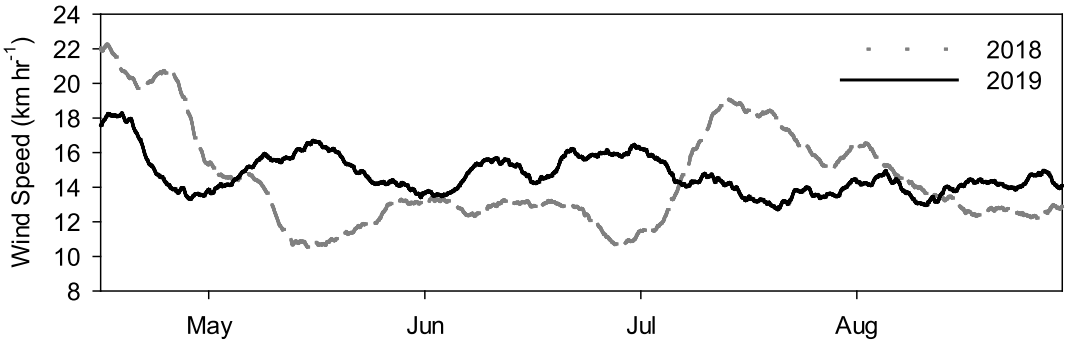

Fig. 7. Wind speed at Redfish Pass RECON in 2018 versus 2019 (10-day moving average).

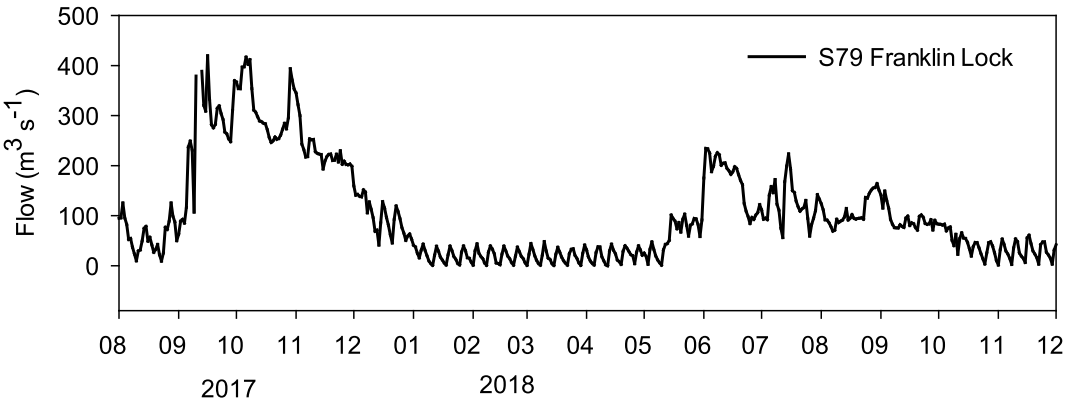

Fig. 8. Flow from Franklin Lock S79 from August 2017 to December 2018. Hurricane Irma made 43 landfall on Sept. 11, 2017; Hurricane Michael passed west of the study area on Oct. 7, 2018.

of 20–30 μg chlorophyll *a* L^{-1} observed in this study. In addition, the lower planktonic algae biomass in the bottom water layer than surface layer observed in this study suggests that the biological oxygen demand responsible for the hypoxia in bottom water involved significant decomposition processes. Many dinoflagellate species can position themselves vertically in the water column through directed swimming behavior (Hasle, 1950; Pearre, 2003). *K. brevis* exhibits a migratory pattern, where populations swim into surface water layers (Kamykowski et al., 1998; Heil et al., 2014b).

It appears that the more important role of the *K. brevis* bloom in this hypoxic event was indirect, namely mass mortalities of marine organisms caused by *K. brevis* toxins (i.e., brevetoxin) (Flewelling et al., 2005; Sipler et al., 2014). Widespread mortalities of invertebrates, fish and marine mammals have been previously observed during intense red tide blooms in the Gulf of Mexico (Smith, 1975; Craig and Crowder, 2005; Smith et al., 2014). The magnitude of the mortality in 2018 is reflected in the amount of dead marine life removed from the beaches of Sanibel Island exceeding 700 mt, and including 271 stranded sea turtles (FWC, 2018). Estimated that hypoxia associated with an intense *Karenia brevis* bloom in 2005 resulted in a 2-3-year recovery period for benthic communities. Dead and decaying biomass on the sea floor associated with HABs, including senescing bloom biomass, increases the potential for hypoxia (CENR, 2010; IWG-HABHRCA, 2016; Pitcher and Probyn, 2016), particularly when limited vertical mixing leads to stratification.

In addition to the hypoxic conditions in the coastal shelf region, continuous dissolved oxygen measurements showed low dissolved oxygen concentrations in semi-enclosed bays (e.g. Tarpon Bay) during spring flood tide periods. During two successive spring tide periods in September 2018, a low oxygen water mass moved past the fixed oxygen sensors near tidal passes during flooding tides. This observation highlights the potential for hypoxic water masses to be transported from the Gulf during into regions of sensitive nearshore biological communities, such as oyster reefs and seagrass beds.

This study demonstrates that the occurrence of HABs become a larger and more intense disturbance to the coastal ocean when coupled with hypoxia. Climate change and increasing anthropogenically-driven eutrophication will likely further increase the distribution, intensity and frequency of HABs and hypoxia in the future (Anderson et al., 2002; Paerl and Paul, 2012; Wells et al., 2015; IWG-HABHRCA, 2016; Griffith and Gobler, 2020). Increased ocean temperatures and changes in weather patterns in areas subject to recurring HABs are expected to make conditions for hypoxia formation more favorable in the future (Griffith and Gobler, 2020). Increased storm frequency and greater nutrient and carbon loads to coastal areas are expected to exacerbate HABs and hypoxia (Diaz and Rosenberg, 2008; Heisler et al., 2008; CENR, 2010; Davidson et al., 2014; IWG-HABHRCA, 2016; Phlips et al., 2020). To be prepared for this future condition, there is a need for expanded continuous monitoring of dissolved oxygen, salinity and temperature through support of an Integrated Ocean Observing System (IOOS) and by supporting regional groups such as GCOOS. Efforts to continuously measure chlorophyll and dissolved oxygen should be expanded in areas with recurring HABs to include autonomous sailing vehicles in addition to distributed sensor networks.

Declaration of competing interest

The authors declare that they have no known competing financial interests or personal relationships that could have appeared to influence the work reported in this paper.

Acknowledgements

This research was funded by the National Science Foundation award 1853041 to N. Nelson, E. Phlips, and E. Milbrandt. RECON operations and maintenance were supported by NOAA through a subaward from the Gulf of Mexico Coastal Ocean Observing Network (GCOOS) to E. Milbrandt. Additional support was provided by the R. Vince Family and Goldman Sachs Gives. Field and lab assistance were provided by student interns from the University of Iowa Department of Earth and Environmental Science. The manuscript was improved by constructive comments from 2 anonymous reviewers.

References

Anderson, D.M., Glibert, P.M., Burkholder, J.M., 2002. Harmful algal blooms and eutrophication: nutrient sources, composision, and consequences. Estuaries 25, 704–726.

Barnes, B.B., Hu, C., Holekamp, K.L., Blonski, S., Spiering, B.A., Palandro, D., Lapointe, B., 2014. Use of Landsat data to track historical water quality changes in Florida Keys marine environments. Remote Sens. Environ. 140, 485–496. https://doi.org/10.1016/j.rse.2013.09.020.

Beckler, J.S., Arutunian, E., Moore, T., Currier, R.D., Milbrandt, E.C., Duncan, S., 2019. Harmful algae bloom monitoring via a sustainable, sail-powered mobile platform for inland and coastal monitoring. Frontiers in Marine Science. https://doi.org/10.3389/fmars.2019.00587.

CENR, 2010. Committee on Environment and Natural Resources. Scientific Assessment of Hypoxia in U.S. Coastal Waters. Interagency Working Group on Harmful Algal Blooms, Hypoxia, and Human Health of the Joint Subcommittee on Ocean Science and Technology, Washington, DC. https://www.whitehouse.gov/sites/default/files/microsites/ostp/hypoxia-report.pdf.

Craig, J.K., Crowder, L.B., 2005. Hypoxia-induced habitat shifts and energetic consequences in atlantic croaker and brown shrimp on the Gulf of Mexico shelf. Mar. Ecol. Prog. Ser. 294, 79–94.

Davidson, K., Gowen, R.J., Harrison, P.J., Flemming, L.E., Hoagland, P., Moschonas, G., 2014. Anthropogenic nutrients and harmful algae in coastal waters. J. Environ. Manag. 146, 206–216.

Diaz, R.J., Rosenberg, R., 2008. Spreading dead zones and consequences for marine ecosystems. Science 321, 926–929.

Fire, S.E., Fauquier, D., Flewelling, L.J., Henry, M., Naar, J., Pierce, R., Wells, R.S., 2007. Brevetoxin exposure in bottlenose dolphins (Tursiops truncates) associated with *Karenia brevis* blooms in Sarasota Bay, Florida. Mar. Biol. 152, 827–834.

Flewelling, L.J., Naar, J.P., Abbott, J.P., Baden, D.G., Barros, N.B., Bossart, G.D., Bottein, M.-Y.D., Hammond, D.G., Haubold, E.M., Heil, C.A., 2005. Brevetoxicosis: red tides and marine mammal mortalities. Nature 435, 755–756.
FWC, 2018. FLSTSSN, Archived Sea Turtle Stranding Data, p. 31.
Gobler, C.J., Doherty, O.M., Hattenrath-Lehmann, T.K., Griffith, A.W., Kang, Y., Litaker, R.W., 2017. Ocean warming since 1982 has expanded the niche of toxic algal blooms in the North Atlantic and North Pacific oceans. Proc. Natl. Acad. Sci. Unit. States Am. 114, 4975–4980.
Griffith, A.W., Gobler, C.J., 2020. Harmful algal blooms: a climate change co-stressor in marine and freshwater ecosystems. Harmful Algae 91, 101590. https://doi.org/10.1016/j.hal.2019.03.008.
Hasle, G.R., 1950. Phototactic vertical migrations in marine dinoflagellates. Oikos 2, 162–175.
He, R., Weisberg, R.H., 2002. West Florida shelf circulation and temperature budget for the 1999 spring transition. Continent. Shelf Res. 22, 719–748.
Heil, C.A., Dixon, L.K., Hall, E., Garrett, M., Lenes, J.M., O'Neil, J.M., Walsh, B.M., Bronk, D.A., Killberg-Thoreson, L., Hitchcock, G.L., Meyer, K.A., Mulholland, M.R., Procise, L., Kirkpatrick, G.J., Walsh, J.J., Weisberg, R.W., 2014a. Blooms of *Karenia brevis* (Davis) G. Hansen & Ø. Moestrup on the West Florida Shelf: nutrient sources and potential management strategies based on a multi-year regional study. Harmful Algae 38, 127–140.
Heil, C.A., Bronk, D.A., Mulholland, M.R., O'Neil, J.M., Bernhardt, P.W., Murasko, S., Havens, J.A., Vargo, G.A., 2014b. Influence of daylight surface aggregation behavior on nutrient cycling during a *Karenia brevis* (Davis) G. Hansen & O. Moestrup bloom: migration to the surface as a nutrient acquisition strategy. Harmful Algae 38, 86–94.
Heisler, J., Glibert, P.M., Burkholder, J.M., Anderson, D.M., Cochlan, W., Dennison, W. C., Dortch, Q., Gobler, C.J., Heil, C.A., Humphries, E., Lewitus, A., Magnien, R., Marshall, H.G., Sellner, K., Stockwell, D.A., Stoecker, D.K., Suddleson, M., 2008. Eutrophication and harmful algal blooms: a scientific consensus. Harmful Algae 8, 3–13. https://doi.org/10.1016/j.hal.2008.08.006.
Howarth, R., Chan, F., Conley, D.J., Garnier, J., Doney, S.C., Marino, R., Billen, G., 2011. Coupled biogeochemical cycles: eutrophication and hypoxia in temperate estuaries and coastal marine ecosystems. Front. Ecol. Environ. 9, 18–26.
Iwg-Habhrca, 2016. Harmful Algal Blooms and Hypoxia Comprehensive Research Plan and Action Strategy: an Interagency Report. Interagency Working Group on the Harmful Algal Bloom and Hypoxia Research and Control Act. National Science and technology Council, Washington, D. C.
Jannasch, H.W., Coletti, L.J., Johnson, K.S., Fitzwater, S.E., Needoba, J.A., Plant, J.N., 2008. The Land/Ocean Biogeochemical Observatory: a robust networked mooring system for continuously monitoring complex biogeochemical cycles in estuaries. Limnol Oceanogr. Methods 263–276.
Kamykowski, D., Milligan, E.J., Reed, R.E., 1998. Relationships between geotaxis/phototaxis and diel vertical migration in autotrophic dinoflagellates. J. Plankton Res. 20, 1781–1796.
Kemp, W.M., Boynton, W.R., Adoli, J.E., Boesch, D.F., Biocourt, W.C., Brush, G., Cornwell, J.C., Fisher, T.R., Glibert, P.M., Hagy, J.D., Harding, L.W., Houde, E.D., Kimmel, D.G., Miller, W.D., Newelll, R.I.E., Roman, M.R., Smith, E.M., Stevenson, J. C., 2005. Eutrophication of Chesapeake Bay: historical trends and ecological interactions. Mar. Ecol. Prog. Ser. 303, 1–29.
Krivorucho, K., Gribov, A., 2019. Evaluation of empirical Bayesian kriging. Spatial Stat. 32 https://doi.org/10.1016/j.spasta.2019.100368.
Landsberg, J.H., Flewelling, L.J., Naar, J., 2009. *Karenia* brevis red tides, brevetoxins in the food web, and impacts on natural resources: decadal advancements. Harmful Algae 8, 598–607.
Menden-Deuer, S., Lessard, E.J., 2000. Carbon to volume relationships for dinoflagellates, diatomsand other protist plankton. Limnol. Oceanogr. 45, 569–579.
Milbrandt, E.C., Coble, P.G., Comny, R.M., Martignette, A.J., Siwicke, J., 2010. Evidence for the production of marine fluorescent dissolved organic matter in coastal environments and a possible mechanism for formation and dispersion. Limnol. Oceanogr. 55, 2037–2051.
Millero, F., Chen, C., Bradshaw, A., Schleicher, K., 1980. A new high pressure equation of state for seawater. Deep Sea Res., Part A 27, 255–264.
Paerl, H.W., Paul, V.J., 2012. Climate change: links to global expansion of harmful cyanobacteria. Water Res. 46, 1349–1363. https://doi.org/10.1016/j.watres.2011.08.002.
Pearre, S., 2003. Eat and run? The hunger/satiation hypothesis in vertical migration: history, evidence and consequences. Biol. Rev. 78, 1–79.
Phlips, E.J., Badylak, S., Hart, J., Haunert, D., Lockwood, J., Manley, H., O'Donnell, K., Sun, D., Viveros, P., Yilmaz, M., 2012. Climatic influences on autochthonous and allochthonous phytoplankton blooms in a subtropical estuary, St. Lucie Estuary, Florida, USA. Estuar. Coast 35, 335–352.
Phlips, E.J., Badylak, S., Lasi, M., Chamberlain, R., Green, W., Hall, L., Hart, J., Lockwood, J., Miller, J., Steward, J., 2015. From red tides to green and brown tides: bloom dynamics in a restricted subtropical lagoon under shifting climatic conditions. Estuar. Coast 38, 886–904. https://doi.org/10.1007/s12237-014-9874-6.
Phlips, E.J., Badylak, S., Nelson, N., Havens, K., 2020. Hurricanes, El Niño and harmful algal blooms in two sub-tropical Florida estuaries: direct and indirect impacts. Sci. Rep. 10, 1910. https://doi.org/10.1038/s41598-020-58771-4.
Pitcher, G.C., Probyn, T.A., 2016. Suffocating phytoplankton, suffocating waters – red tides and anoxia. Frontiers in Marine Science 3, 186. https://doi.org/10.3389/fmars.2016.00186.
Rabalais, N.N., Turner, R.E., 1994. Comparison of continuous records of near-bottom dissolved oxygen from the hypoxia zone along the Louisiana coast. Estuaries 17, 850–861.
Rabalais, N.N.R.E., Turner, B.K. Sen, Gupta, Boesch, D.F., Chapman, P., Murrell, M.C., 2007. Characterization and long-term trends of hypoxia in the northern Gulf of Mexico: does the science support the Action Plan? Estuar. Coast 30, 753–772.
Rabalais, N.N., Cai, W.J., Carstensen, J., conley, D.J., Fry, B., Quinones-Rivera, X., Rosenberg, R., Slomp, C.P., Turner, R.E., Voss, M., Wissel, B., Zhang, J., 2014. Eutrophication-driven deoxygenation in the coastal ocean. Oceanography 70, 123–133.
Scavia, D., Rabalais, N.N., Turner, R.E., Justic, D., Wiseman Jr., W.J., 2003. Predicting the response of Gulf of Mexico hypoxia to variations in Mississippi River nitrogen load. Limnol. Oceanogr. 48, 951–956.
Scavia, D., Allan, J.D., Arend, K.K., Bartel, S., Beletsky, D., Bosch, N.S., Brandt, S.B., Briland, R.D., Daloğlu, I., DePinto, J.V., Dolan, D.M., Evans, M.A., Farmer, T.M., Goto, D., Han, H., Höök, T.O., Knight, R., Ludsin, S.A., Mason, D., Michalak, A.M., Richards, R.P., Roberts, J.J., Rucinski, D.K., Rutherford, E., Schwab, D.J., Sesterhenn, T.M., Zhang, H., Zhou, Y., 2014. Assessing and addressing the re-eutrophication of Lake Erie: central basin hypoxia. J. Great Lake. Res. 40, 226–246.
Sipler, R.E., McGuinness, L.R., Kirkpatrick, G.J., Kerkhof, L.J., Schofield, O.M., 2014. Bacteriocidal effects of brevetoxin on natural microbial communities. Harmful Algae 38, 101–109.
Smith, G.B., 1975. The 1971 red tide and its impact on certain reef communities in the mid-eastern Gulf of Mexico. Environ. Lett. 9, 141–152.
Smith, M.D., Asche, F., Bennear, L.S., Oglend, A., 2014. Spatial-Dynamics of hypoxia and fisheries: the case of Gulf of Mexico Brown shrimp. Mar. Resour. Econ. 29, 111–131.
Smith, D.R., King, K.W., Williams, M.R., 2015. What is causing the harmful algal blooms in Lake Erie. J. Soil Water Conserv. 70, 27A–29A.
Stow, C.A., Qian, S.S., Craig, J.K., 2005. Declining threshold for hypoxia in the Gulf of Mexico. Environ. Sci. Technol. 39, 716–723.
Tester, P.A., Steidinger, K.A., 1997. *Gymnodinium breve* red tide blooms: initiation, transport, and consequences of surface circulation. Limnol. Oceanogr. 42, 1039–1051.
Tomasko, D.A., Anastasiou, C., Kovach, C., 2006. Dissolved oxygen dynamics in Charlotte harbor and its contributing watershed, in response to hurricanes charley, frances, and jeanne – impacts and recovery. Estuar. Coast 29, 932–938.
Turner, R.E., Rabalais, N.N., Fry, B., Atilla, N., Milan, C.S., Lee, J.M., Normandeau, C., Oswald, T.A., Swenson, E.M., Tomasko, D.A., 2006. Paleo-indicators and water quality change in the Charlotte Harbor estuary (Florida). Limnol. Oceanogr. 51, 518–533.
Urquhart, E.A., Schaeffer, B.A., Stumpf, R.P., Loftin, K.A., Werdell, P.J., 2017. A method for examining temporal changes in cyanobacterial harmful algal bloom spatial extent using satellite remote sensing. Harmful Algae 67, 144–152. https://doi.org/10.1016/j.hal.2017.06.001.
Utermöhl, H., 1958. Zur Vervollkommnung der quantitativen phytoplankton-methodik. Mitt. Int. Ver. Theor. Angew. Limnol. 9, 1–38.
Vaquer-Sunyer, R., Duarte, C.M., 2008. Thresholds of hypoxia for marine biodiversity. Proc. Natl. Acad. Sci. Unit. States Am. 105, 15452–15457.
Vargo, G.A., 2009. A brief summary of the physiology and ecology of *Karenia brevis* Davis (G. Hansen and Moestrup comb nov.) red tides on the West Florida Shelf and of hypotheses posed for their initiation, growth, maintenance and termination. Harmful Algae 8, 573–584.
Vargo, G.A., Carder, K.L., Gregg, W., Shanley, E., Heil, C., 1987. The potential contribution of primary production by red tides to the west Florida shelf ecosystem. Limnol. Oceanogr. 32, 762–767.
Watson, S.B., Miller, C., Arhonditsis, G., Boyer, G.L., Carmichael, W., Charlton, M.N., Confesor, R., Depew, D.C., Höök, T.O., Ludsin, S.A., Matisoff, G., McElmurry, S.P., Murray, M.W., Richards, R.P., Rao, Y.R., Steffen, M.M., Wilhelm, S.W., 2016. The re-eutrophication of Lake Erie: harmful algal blooms and hypoxia. Harmful Algae 56, 44–66.
Weisberg, R.H., Barth, A., Alvera-Azcarate, A., Zheng, L., 2009. A coordinated coastal ocean observing and modeling system for the West Florida Continental Shelf. Harmful Algae 8, 585–597.
Wells, M.L., Trainer, V.L., Smayda, T.J., Karlson, B.S.O., Trick, C.G., Kudela, R.M., Ishikawa, A., Bernard, S., Wulff, A., Anderson, D.M., Cochlan, W.P., 2015. Harmful algal blooms (HABs) and climate change: what do we know and where do we go from here? Harmful Algae 49, 68–93.
Zhang, J.D., Gilbert, A.J., Gooday, L., Levin, S.W.A., Naqvi, J.J., Middleburg, M., Scranton, W., Ekau, A., Pena, B., Dewitte, T., Oguz, P.M.S., Monteiro, E., Urban, N. N., Rabalais, V., Ittekot, W.M., Kemp, O., Ulloa, R., Elmgren, E., Escobar-Briones, A. K. Van der Plas, 2010. Natural and human-incuced hypoxia and consequences for coastal areas: synthesis and future development. Biogosciences 7, 1443–1467.